THE JOURNAL OF PHYSICAL CHEMISTRY B

Article

pubs.acs.org/JPCB

Thermodynamic Properties of Hydration Water around Solutes: Effect of Solute Size and Water−Solute Interaction

A. Oleinikova* and I. Brovchenko

Physical Chemistry, Dortmund University of Technology, Otto-Hahn-Str. 6, Dortmund, D-44227, Germany

ABSTRACT: Density, thermal expansion, and heat capacity of hydration water around various model solutes have been studied as a function of temperature and pressure. The radius of spherical structureless solute was varied from 3 to 10 Å, and the water−solute interaction was varied from strongly hydrophobic to strongly hydrophilic. Thermodynamic properties of hydration water around solutes were compared with those near the inner surface of large cylindrical pores with a radius of 25 Å. For all systems studied, the energy of water−water interactions per molecule in the hydration shell is found less negative than in the bulk. This is the result of the missing neighbor effect, which leads to the liquid density depletion even near strongly hydrophilic surfaces. This effect enhances near concave surfaces and diminishes near convex surfaces, which causes an essential increase of hydration water density around small solutes. Liquid density depletion near surfaces is accompanied by an essential increase of the thermal expansion coefficient of hydration water: at low temperatures, it exceeds the bulk value even near strongly hydrophilic surfaces. The constant volume heat capacity of hydration water is close to the bulk value; it is practically not sensitive to water−surface interaction and slightly increases upon decreasing solute size. The constant pressure heat capacity of hydration water increases upon weakening water−surface interaction and is practically not sensitive to solute size. Increase of the constant pressure heat capacity of water near hydrophobic surfaces is found to be the result of the increasing thermal expansion coefficient.

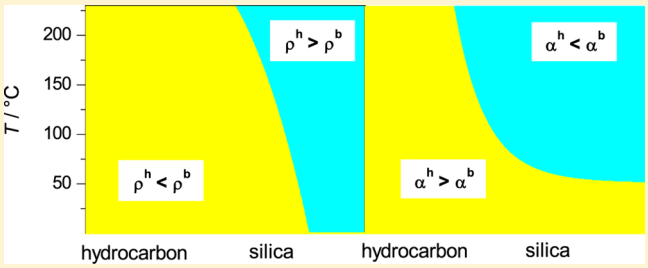

I. INTRODUCTION

Thermodynamic properties of fluids (density, heat capacity, etc.) are local in the presence of a surface. Far from the liquid−vapor critical point, the intrusion of the surface perturbation into the bulk fluid is noticeable in close proximity of a surface only. In particular, properties of liquid water differ strongly from the bulk ones in the first surface layer (hydration water), the difference is still noticeable in the second layer, and it is practically absent further from the surface.[1] Hydration water makes an important contribution to the properties of various aqueous systems (confined water, aqueous solutions, etc.), and therefore, it is important to know the thermodynamic properties of hydration water and their dependence on the surface characteristics.

In low-hydrated systems, where most of the water molecules are presumably adsorbed at the surface, the properties of hydration water can be estimated experimentally from the difference in the properties of hydrated and dry systems.[2,3] It is much more difficult to measure experimentally properties of hydration water in systems with high water content (liquid water near extended surfaces, aqueous solutions, completely filled mesopores, etc.). Some nondirect information about the thermodynamic properties of hydration water can be obtained from the measurements of the average properties of aqueous systems. For example, the average density and the average thermal expansion coefficient of confined water differ from the respective bulk values[4−8] and this difference gains more importance in smaller pores, where the fraction of hydration water is larger.[6,5] The experiments on dissolution of organic molecules in liquid water evidence that the hydration contribution to the constant pressure heat capacity is positive for apolar groups and negative for polar and charged groups.[9,10] More direct information about the profiles of hydration water can be obtained using reflectivity and diffraction techniques. For example, the reflectivity measurements evidence the depletion of liquid water density near extended hydrophobic surfaces and allow estimation of the total water density deficit near a surface.[11−13] The density profile of liquid water near a hydrophilic surface has been obtained from the reflectivity data assuming an oscillating shape of the profile.[14] Use of the simulation technique ("empirical potential structure refinement") for the analysis of the experimental diffraction data allows estimation of the density profiles of water in narrow silica pores.[15,16] Such experimental studies of liquid water density near surfaces are rather rare, and we are not aware of the direct experimental studies of liquid water thermal expansivity or heat capacity near surfaces.

The local properties of fluids near surfaces can be studied in detail by simulations. To simulate a liquid near a surface, it should be confined in pore geometry with periodic boundary conditions in up to two dimensions and the pore should be large enough to minimize the shift of the liquid−vapor phase

Received: July 9, 2012
Revised: October 19, 2012
Published: November 21, 2012

transition due to confinement. Alternatively, some object should be placed in a bulk liquid (with periodic boundary conditions in three dimensions). The *liquid density profiles* have been reported in numerous simulation studies of liquid water near various surfaces. The main features of the profiles are quite similar to those of other liquids: oscillating shape, increasing density near a surface upon strengthening fluid−surface interaction, upon increasing pressure, or decreasing temperature. The effect of the solute size on the density profiles of liquid water has been studied for various systems: cavities,[17,18] hard and purely repulsive solutes,[19−26] and weakly attractive solutes[22,25−28] in liquid water. In all cases, a decrease of solute size causes an increase of water density near a solute. Note that the average value of liquid water density in hydration shell ρ^1 is usually not reported in simulation studies. The calculation of ρ^1 requires a physically reasonable determination of the volume of hydration shell and of the distance to a surface, which is not easy, especially in the case of structured surfaces and complicated water−surface potentials.

Other thermodynamic properties of liquid water near surfaces are much less studied. The thermal expansion coefficient of hydration water α_p^1 has been studied in cylindrical pores with structureless surfaces: α_p^1 exceeds the bulk value for hydrophobic and moderately hydrophilic surfaces and shows a radically different temperature dependence.[29] α_p^1 in hydration shells of various biomolecues[30−32] has been found quite similar to that near moderately hydrophilic structureless surfaces. The constant pressure heat capacity of hydration water C_p^1 was studied near small hydrophobic solutes, and its essential enhancement with respect to the bulk value was observed.[33−35] All-atomic simulations of polypeptides in liquid water show that C_p^1 exceeds the bulk value by ∼0.27 cal mol^{-1} K^{-1} near hydrophilic peptide and by ∼1.3 cal mol^{-1} K^{-1} near hydrophobic peptide in a wide temperature range.[36] Isothermal compressibility of hydration water near hydrophobic solutes increases with increasing solute size and decreases upon strengthening water−solute interaction.[26]

Thus, many questions concerning the relation between the thermodynamic properties of hydration water and the surface properties remain unanswered. The range of the possible variations of the density and the thermal expansion coefficient of hydration water with respect to the bulk values is still not clear. The effect of the solute size and water−solute interaction on the thermal expansion coefficient and heat capacity of hydration water has not been studied yet. In the present paper, we perform systematic studies of the effect of water−solute interaction and solute size on the density, thermal expansion coefficient, and heat capacity of hydration water near structureless attractive spherical solutes. To clarify the effect of surface curvature on the properties of hydration water, similar studies have been performed also for water near concave cylindrical surfaces. The specific peculiarities of hydration water have been clarified by comparison with the properties of Lennard-Jones (LJ) fluids near surfaces.

II. METHODS

Thermodynamic properties of hydration water near structureless spherical solutes were studied by Monte Carlo (MC) simulations of TIT4P[37] water with a spherical cutoff of 8.5 Å for both the Coulombic and LJ parts of the water−water interaction potential. In accordance with the original parametrization of the TIP4P model, no long-range corrections were included. The thermodynamic properties of bulk TIT4P water have already been extensively studied. In particular, its liquid−vapor coexistence has been simulated[38] and the chemical potential of liquid water along this coexistence has been calculated.[39] In the present paper, we have calculated additionally the constant pressure and constant volume heat capacities of bulk liquid TIP4P water. This has been done by MC simulations of the systems with 512 molecules in the constant volume ensemble at 32 temperatures from T = 270 to 580 K along the liquid−vapor coexistence curve.

The spherical solutes of various radii were fixed in the center of the cubic simulation box, which includes 1500 water molecules. MC simulations of such systems were performed in the constant pressure ensemble at p = 1 bar to 5 kbar and T = 270−420 K. The box size varied within about 36−39 Å for systems with spherical solutes. Thermodynamic properties of hydration water near a concave cylindrical surface were studied by constant-volume MC simulations of TIP4P water in five cylindrical pores of a radius R_c = 25 Å and length 50 Å along their respective liquid−vapor pore coexistence curves. At the lowest temperature studied (T = 270 K), the simulated system was composed of ∼2800 to ∼3000 water molecules in the strongly hydrophobic pore and the strongly hydrophilic pore, respectively. The volumetric properties of water in these pores have been reported in ref 29. Additionally, we used the results of the simulations of liquid water in the cylindrical pore of a radius R_c = 12 Å and in the spherical pore of a radius R_s = 20 Å.[40] In those studies, confined water was simulated in equilibrium with external saturated bulk water.

The interaction between the water molecules and the model solute was described by a (9−3) LJ potential:

$$U_{ws}(r) = \varepsilon[(\sigma/r)^9 - (\sigma/r)^3] \quad (1)$$

where r is the distance from the water oxygen to the solute surface and σ = 2.5 Å. The parameter ε in eq 1 was chosen to mimic a strongly hydrophobic paraffin-like surface with the well-depth U_0 = −0.39 kcal/mol, a moderately hydrophilic biological-like surface with U_0 = −1.93 kcal/mol,[36] and a strongly hydrophilic metallic-like surface with U_0 = −4.62 kcal/mol. The effect of water−solute interaction on hydration water was studied by the simulations of three solutes with R_s = 10 Å and with the well-depths U_0 mentioned above with the temperature step 10 K at p = 1 bar. Four spheres with the radii R_s = 10, 7.5, 5, and 3 Å and with U_0 = −1.93 kcal/mol were simulated at the same thermodynamic states to study the effect of the solute size on hydration water. The impact of pressure was evaluated by simulations of the isotherm T = 300 K at 15 different pressures in the interval from p = 1 bar to p = 5 kbar and three isobars p = 1 bar, 1 kbar, and 5 kbar with the temperature step 10 K for the solute with R_s = 10 Å and U_0 = −1.93 kcal/mol. MC simulations of water properties in cylindrical pores were performed in the temperature interval from 270 to 420 K with the temperature step 5 K under conditions of the liquid−vapor equilibrium in pores.[41]

Simulations of the volumetric properties of LJ liquid near surfaces were performed for LJ fluids confined in slit pores with a width 12 σ along the respective pore liquid−vapor coexistence curves. The simulations of LJ fluid in the pore with the weak fluid−surface interaction, characterized by the coefficient f = 0.3, have been reported in ref 42. In a similar way, we have simulated the liquid−vapor coexistence curves for the fluid−surface interaction with f = 0.644, which corresponds to the conditions of a "neutral wall"[43,44] (see below), and with f = 1

dx.doi.org/10.1021/jp306781y | J. Phys. Chem. B 2012, 116, 14650−14659

and f = 2 (the details of these studies will be published elsewhere).

III. RESULTS

A. Density of Hydration Water. The selected water density profiles $\rho(r)$ near spherical solutes with R_s = 10 Å at various temperatures and pressures and near an inner surface of cylindrical pore R_c = 25 Å are shown in Figure 1. The first

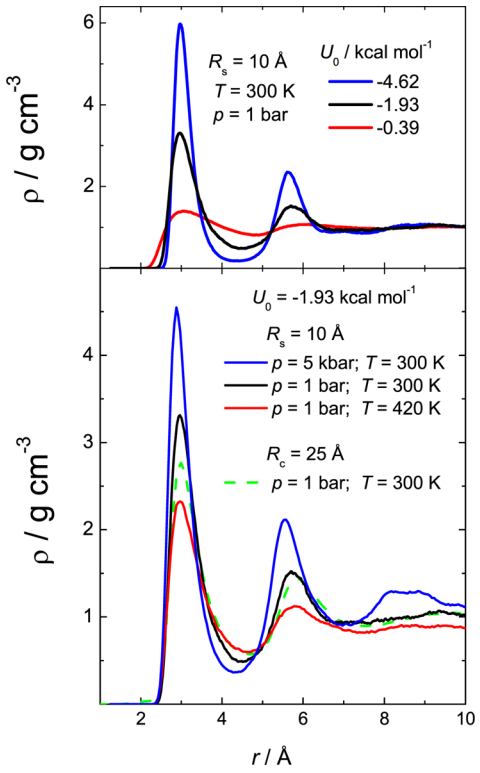

Figure 1. Upper panel: effect of water−solute interaction U_0 on the density profile of liquid water near solutes. Lower panel: effect of temperature, pressure, and surface curvature on the density profiles of liquid water.

maximum of $\rho(r)$ at $r \approx 3$ Å indicates localization of water molecules in the well of the water−surface potential given by eq 1. The height of this maximum ρ_{max} increases upon strengthening water−surface interaction (Figure 2, upper panel), upon increasing pressure and decreasing temperature (Figure 2, middle panel), and upon decreasing surface curvature $1/R$, which is $1/R_s$ for the convex spherical surface, $-1/R_s$ for the concave spherical surface, and $-1/2R_c$ for the concave cylindrical surface (Figure 2, lower panel). The dependences shown in Figure 2 qualitatively agree with the previous studies of water density profiles around various objects.[17−22,24−26,28] A non-monotonous dependence $\rho_{max}(R^{-1})$ for large R^{-1} can reflect specific packing of water molecules around small solutes.

The knowledge of the average density of water in the hydration shell ρ^1 allows distinguishing the regimes of liquid density depletion or enchanecement near a surface by comparison of ρ^1 with the liquid water density ρ^b. The first minimum of $\rho(r)$ at $r \approx 4.5$ Å only slightly depends on water−surface interaction, temperature, and pressure and can be considered as an outer border of the first hydration shell. Water−surface interaction is equal to zero, when the distance

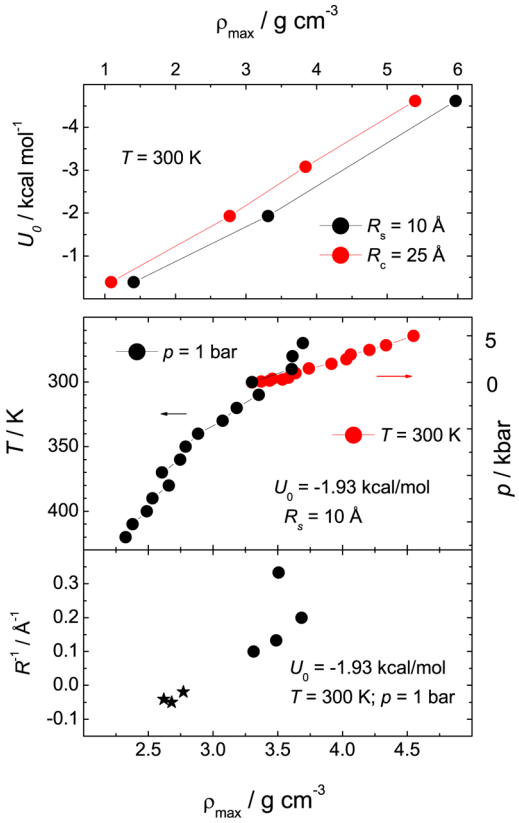

Figure 2. Effect of various factors on the height ρ_{max} of the first maximum of the density profiles of liquid water. Upper panel: effect of water−solute interaction U_0. Middle panel: effect of temperature and pressure. Lower panel: effect of surface curvature.

between the centers of surface atoms and water oxygen atoms is 2.5 Å, and it is reasonable to divide equally this space interval between a solid and a fluid. Thus, the density of hydration water ρ^1 was calculated as an integral of $\rho(r)$ from r = 1.25 Å to r = 4.5 Å. The average water density in the second hydration shell ρ^2 was calculated by the integration of the density profile from r = 4.5 Å to r = 7.5 Å.

The obtained temperature dependences of ρ^1 are shown in Figure 3: ρ^1 increases upon strengthening water−solute interaction (upper panel), decreasing solute size (increasing curvture $1/R$, middle panel), and increasing pressure (lower panel). All these trends are qualitatively the same, as for ρ_{max} (Figure 2). It is not surprising, as ρ^1 closely correlates with ρ_{max} (Figure 4a). The dependences in Figure 4b show how ρ^1 can deviate from the bulk value ρ^b upon almost the largest possible variation of water−solute interaction. At T = 300 K, ρ^1 near solutes with R_s = 10 Å is by ∼10% above the bulk value for strongly hydrophilic solute and is by ∼20% below the bulk value for strongly hydrophobic solute, and these changes become more pronounced at higher temperatures. Similar changes of ρ^1 upon varying U_0 have been observed for water near an inner surface of cylindrical pores.[29] Water density in the second hydration shell is essentially closer to the bulk one and shows weak dependence on U_0 (Figure 4b). A decrease of the solute size to R_s = 3 Å causes an increase of ρ^1 by ∼15% with respect to the planar surface with the same U_0 (Figure 4c). An increase of pressure from 1 bar to 5 kbar at T = 300 K densifies the hydration water by more than 10% (Figure 4d), and this effect becomes more pronounced upon heating. The compressibility of water near a moderately hydrophilic surface

dx.doi.org/10.1021/jp306781y | J. Phys. Chem. B 2012, 116, 14650−14659

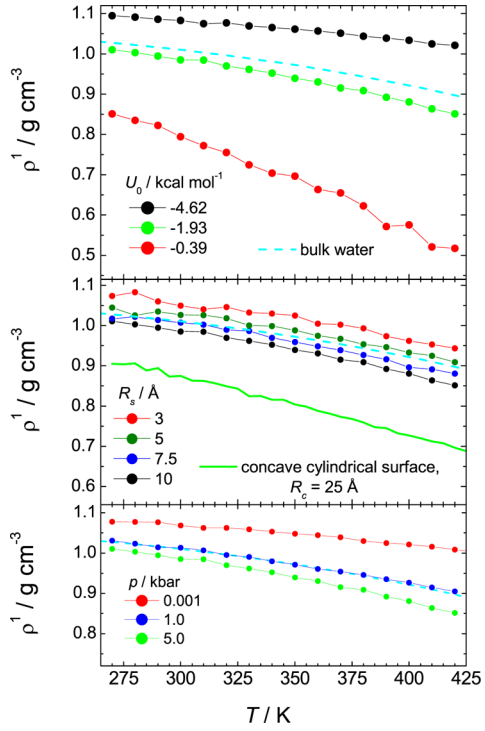

Figure 3. Density of hydration water ρ^1 near various solutes as a function of temperature. Upper panel: R_s = 10 Å, p = 1 bar; middle panel: U_0 = −1.93 kcal/mol; lower panel: R_s = 10 Å, U_0 = −1.93 kcal/mol.

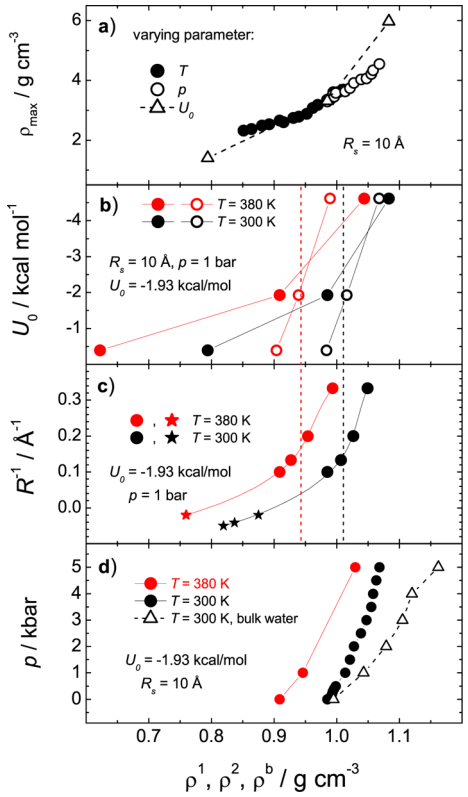

Figure 4. (a) Correlations between ρ_{max} and the density of hydration water ρ^1 in the course of varying temperature (U_0 = −1.93 kcal/mol, p = 1 bar), pressure (U_0 = −1.93 kcal/mol, T = 300 K), or water−solute interaction (p = 1 bar, T = 300 K). (b) Effect of water−solute interaction U_0 on water density in the first (ρ^1, closed symbols) and second (ρ^2, open symbols) hydration shells. (c) Effect of the surface curvature R^{-1} on ρ^1: convex sperical surfaces of various radii (circles), concave cylindrical surfaces of radii R_c = 25 and 12 Å, and concave spherical surface of radius R_s = 20 Å (stars). (d) Effect of pressure on ρ^1 (circles) and on the density of bulk liquid water ρ^b (triangles[57]). The bulk densities of liquid water ρ^b at p = 1 bar are shown by dashed vertical lines for two temperatures.

decreases (compare the pressure dependence of ρ^1 and ρ^b in Figure 4c). Note that increase of liquid water compressibility has been observed near strongly hydrophobic solutes.[26]

B. Thermal Expansion Coefficient. The temperature dependences of ρ^1 have been fitted by third order polynomial function for solutes with R_s = 10 Å and by second order polynomial function for smaller solutes. The thermal expansion coefficient of hydration water α_p^1 was calculated using the derivative $\partial\rho^1/\partial T$ of the polynomial fits as

$$\alpha_p^1 = -\frac{1}{\rho^1}\frac{\partial\rho^1}{\partial T} \qquad (2)$$

The thermal expansion coefficient of the bulk liquid water was calculated in a similar way.

α_p^1 near spherical solutes strongly depends on the water−solute interaction. It is rather close to that of bulk water for the moderately hydrophilic surface with U_0 = −1.93 kcal/mol and strongly increases near hydrophobic surfaces (Figure 5, upper panel). This agrees with the previous studies of hydration water near concave cylindrical surfaces.[29] A slight decrease of α_p^1 is observed upon decreasing solute size and upon increasing pressure (Figure 5). The thermal expansion coefficient of hydration water closely anticorrelates with its density: a decrease of ρ^1 upon heating or upon weakening water−surface interaction causes an increase of α_p^1 (Figure 6, upper panel).

C. Interaction Energy of Hydration Water. The total potential energy E_{tot}^1 of hydration water includes the energy of interaction with neighbors in the hydration shell E_{hh}^1, the energy of interaction with water outside the hydration shell E_{hb}^1, and the direct water−surface interaction E_s. The overall energy of water−water interaction for hydration water $E_{ww}^1 = E_{hh}^1 + E_{hb}^1$ near all studied convex and concave surfaces was found less negative than the energy of water−water interaction E_{ww}^b in bulk liquid water at the same temperature (Figure 7). There is a clear anticorrelation between E_{ww}^1 and the density of hydration water: ρ^1 increases practically linearly, when E_{ww}^1 decreases due to increasing pressure or strengthening water−surface interaction at constant temperature (Figure 6, lower panel). The dependence $\rho^1(E_{ww}^1)$ is weaker, when E_{ww}^1 changes due to the variation of the surface curvature. Increase of ρ^1 due to strengthening water−surface interaction (Figure 7, left panel), increasing surface curvature (Figure 7, middle panel), and increasing pressure (Figure 7, right panel) cannot compensate the missing neighbor effect, and E_{ww}^1 always exceeds E_{ww}^b. In the second hydration shell, the total potential energy of water−water interactions is essentially closer to that of bulk liquid water (Figure 7, left panel).

Strengthening water−solute interaction affects the constituents of E_{ww}^1, E_{hh}^1 and E_{hb}^1, in different ways. E_{hh}^1 decreases whereas E_{hb}^1 increases upon strengthenning water−solute interaction (Figure 8, left panels). Thus, increase of hydration water density near hydrophilic surfaces improves water−water interactions within the hydration shell but worsens interactions of hydration water with water outside the hydration shell. The effect of the surface curvature on E_{hh}^1 and E_{hb}^1 is quite different.

dx.doi.org/10.1021/jp306781y | J. Phys. Chem. B 2012, 116, 14650−14659

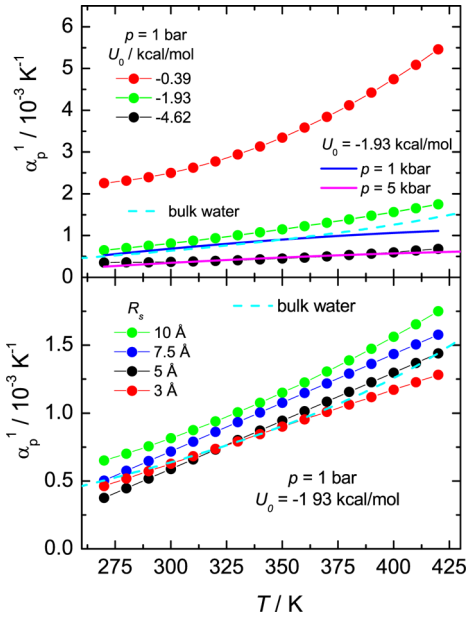

Figure 5. Upper panel: thermal expansion coefficient α_p^1 of hydration water near solutes with R_s = 10 Å. Lower panel: α_p^1 of hydration water near solutes with different radii. α_p for bulk water is shown by dashed lines.

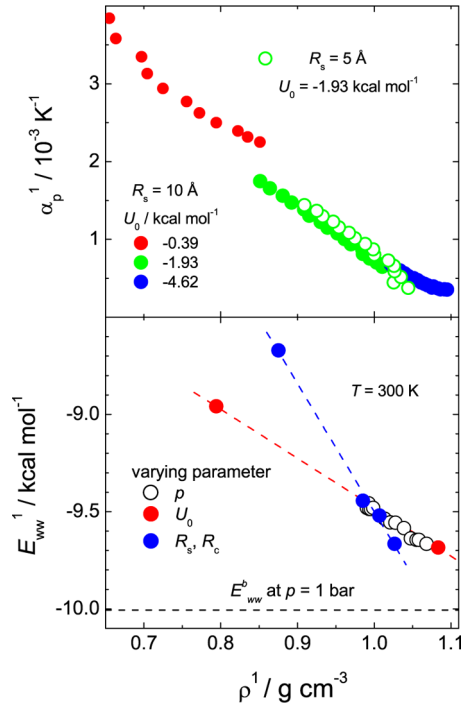

Figure 6. Upper panel: Dependence of the thermal expansion coefficient of hydration water α_p^1 near spherical solutes on its density ρ^1. Lower panel: correlation between the energy of water−water interactions per one molecule in the hydration shell E_{ww}^1 and the density of hydration water ρ^1 near solutes with R_s = 10 Å in the course of varying U_0 (p = 1 bar), pressure (U_0 = −1.93 kcal/mol), and near various surfaces upon varying surface curvature (U_0 = −1.93 kcal/mol, p = 1 bar).

The water−water interaction within the hydration shell E_{hh}^1 is almost not sensitive to the solute size (Figure 8, right upper panel). Even a change from a spherical convex surface to a cylindrical concave surface affects E_{hh}^1 only slightly. In contrast, interaction of hydration water with water outside the hydration shell, E_{hb}^1, continuously decreases upon increasing surface curvature (Figure 8, right lower panel).

D. Heat Capacity of Hydration Water. The constant pressure molar specific heat C_p^1 of hydration water was calculated from the temperature dependence of its total potential energy:

$$C_p^1 = \left(\frac{\partial E_{tot}^1}{\partial T}\right)_p + pV\alpha_p + RT \tag{3}$$

The first term in eq 3 was calculated by numerical differentiation followed by five-point smoothing in order to reduce the scattering of the data points. The contribution of the second term in eq 3 never exceeded 0.05%. Additionally, the heat capacity C_p was simulated in the second and third hydration layers in the systems with spherical solutes. The constant pressure heat capacity C_p^b of the bulk liquid water was calculated similarly by the differentiation of the temperature dependence of E_{ww}^b for liquid water along the liquid−vapor coexistence curve.[38,39] The obtained temperature dependence of C_p^b is shown in Figure 9 (upper panel) together with the experimental data.[45] The main difference between the simulated and experimental dependences originates from the fact that the liquid−vapor critical temperature of TIP4P water is about 60° below the experimental value.[38]

The water−solute interaction affects notably C_p^1 near both convex and concave surfaces (Figure 10). The constant pressure specific heat of hydration water near a strongly attractive surface with U_0 = −4.62 kcal/mol is in general slightly below the bulk value C_p^b and exceeds C_p^b by a few percent near surfaces with U_0 = −1.93 kcal/mol and by up to 20% near hydrophobic surfaces with U_0 = −0.39 kcal/mol. A similar but weaker trend is clearly seen also for the constant pressure specific heat of water in the second hydration shell C_p^2 (Figure 10, middle panel). Note that the deviation of C_p^2 from C_p^b near hydrophobic solute increases upon heating. The heat capacity of water in the third layer does not differ from C_p^b within accuracy of simulations. An increase of pressure from 1 bar to 5 kbar causes a decrease of C_p^1 by about 10% at low temperatures (not shown). We have found C_p^1 indistinguishable near the solutes with different radii but with the same U_0. Moreover, the change of the surface curvature from convex to concave practically does not affect C_p^1, as is seen from Figure 11 (upper panel).

The constant volume molar specific heat of bulk liquid water, C_v^b, was calculated in the constant volume ensemble for various temperatures along the liquid−vapor coexistence using fluctuations of molar interaction energy ΔE_b of the bulk liquid water

$$C_v^b = \frac{N}{RT^2}\langle(\Delta E_{ww}^b)^2\rangle + 3R \tag{4}$$

and the obtained temperature dependence is shown in Figure 9 (lower panel) together with the experimental data.[45] The hydration shell is a constant-volume system, which allows an exchange of water molecules between the hydration shell and the rest of water. Therefore, the thermodynamic properties in the hydration shell can be calculated as in the grand canonical ensemble. The constant-volume molar specific heat C_v^1 of hydration water was calculated as

dx.doi.org/10.1021/jp306781y | J. Phys. Chem. B 2012, 116, 14650−14659

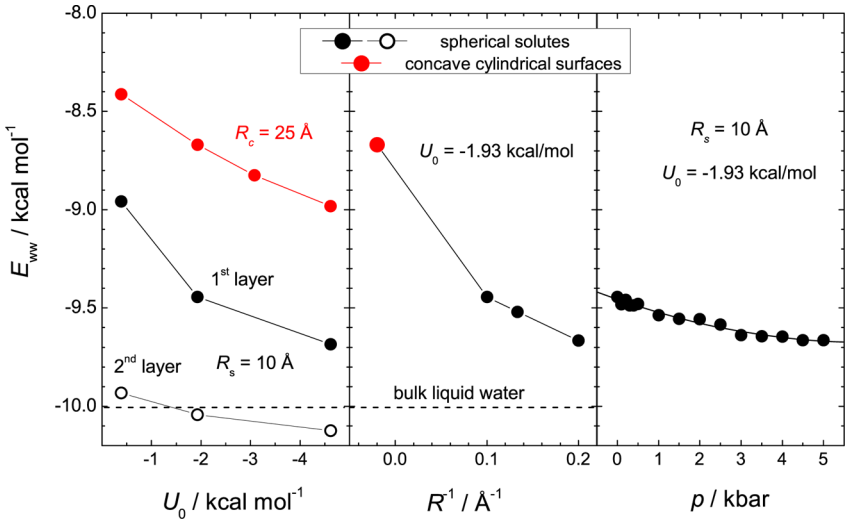

Figure 7. Effect of various factors on the water−water interaction energy E^1_{ww} in the first and second hydration water shells at T = 300 K. The water−water interaction energy for bulk water E^b_{ww} is indicated by a dashed line.

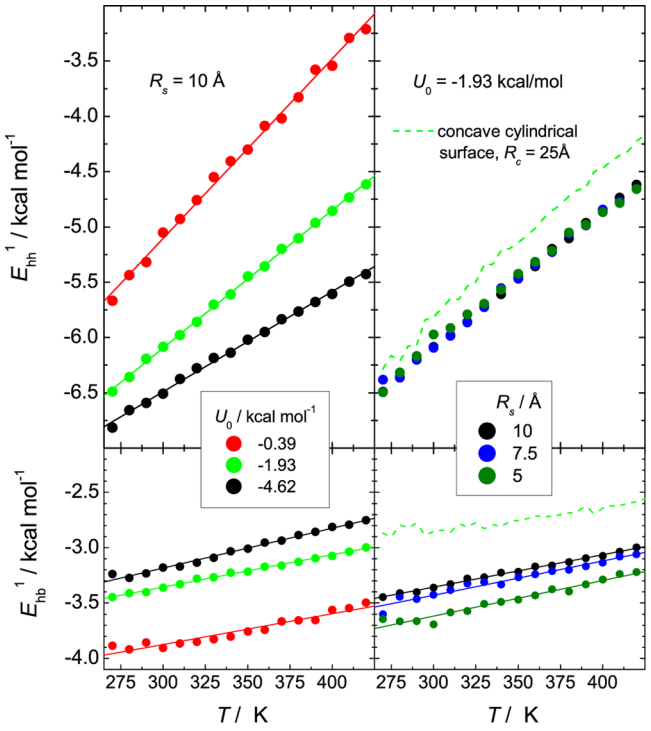

Figure 8. Temperature dependences of the potential energy of interaction within hydration shell E^1_{hh} (upper panels) and between hydration and bulk water E^1_{hb} (lower panels) near spherical solutes (symbols) and near concave cylindrical surfaces (dashed lines). Linear fits of the simulated data are shown by thin solid lines.

$$C_v^1 = \frac{1}{NRT^2}\left[\langle(\Delta E^1_{tot})^2\rangle - \frac{\langle \Delta E^1_{tot}\Delta N\rangle^2}{\langle \Delta N^2\rangle}\right] + 3R \qquad (5)$$

where ΔN and ΔE^1 are the fluctuations of the number of water molecules and of the molar total interaction energy in the hydration shell. The obtained temperature dependences of C_v^1 are shown in Figure 12 for various water−surface interactions U_0. Contrary to the constant-pressure specific heat, C_v^1 is not sensitive to the water−surface interaction for spherical solutes as well as for concave cylindrical surfaces. The temperature

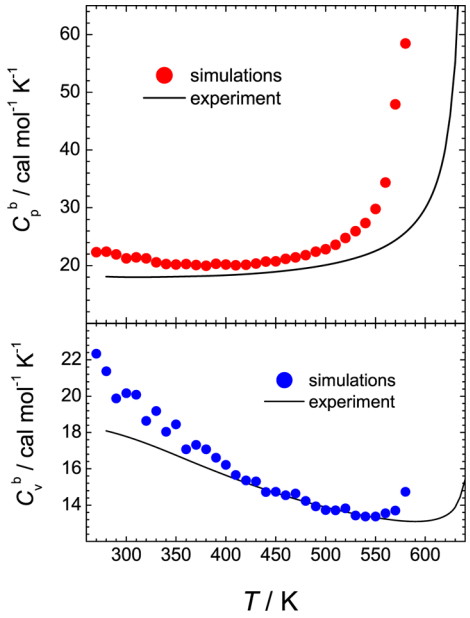

Figure 9. The molar bulk heat capacities C_p^b and C_v^b of model TIP4P water at various temperatures calculated along the liquid−vapor coexistence curve in the present paper and those of real liquid water.[45]

dependences of C_v^1 for water near a large concave cylindrical surface and near a small convex spherical surface with U_0 = −1.93 kcal/mol (Figure 11, lower panel) show a slight increase of C_v^1 upon increasing surface curvature. The effect of pressure on C_v^1 was found to be negligible for pressures up to 1 kbar. Upon a further increase of pressure up to p = 5 kbar, C_v^1 slightly decreases (not shown).

IV. DISCUSSION

We have performed systematic simulation studies of liquid water near various structureless surfaces in order to clarify the effects of water−surface interaction and surface curvature on density, thermal expansivity, and heat capacity of hydration water. The practically relevant range of water−surface attraction is limited from the hydrophobic side by a "hard wall" and, from another side, by strongly hydrophilic surfaces,

dx.doi.org/10.1021/jp306781y | J. Phys. Chem. B 2012, 116, 14650−14659

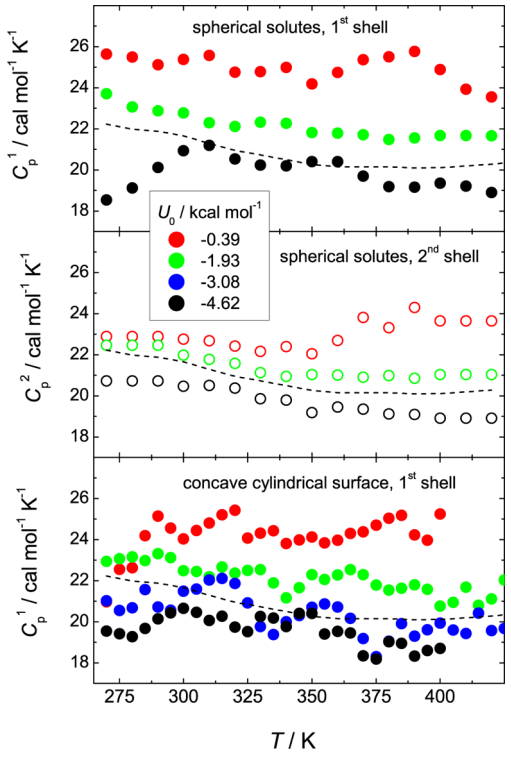

Figure 10. Temperature dependences of the specific heat C_p^1 of hydration water near spherical solutes of radius R_s = 10 Å (upper panel) and concave cylindrical surfaces with R_c = 25 Å (lower panel) for various water−surface interactions U_0. The specific heat of water in the second water layer near spherical solutes is shown in the middle panel.

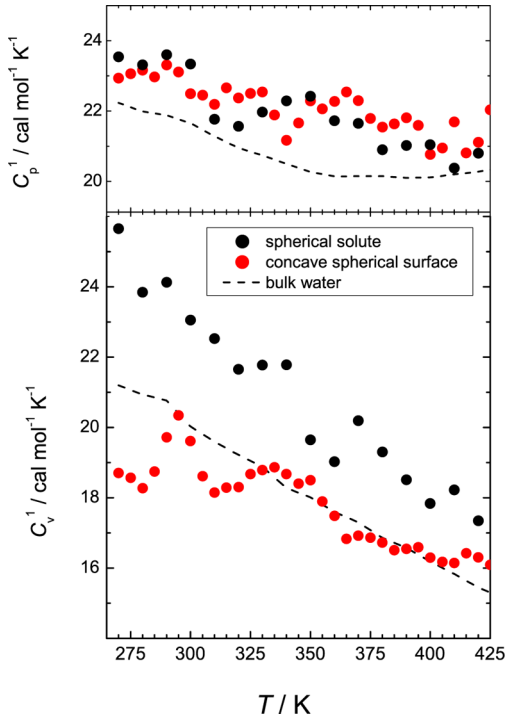

Figure 11. Comparison of the temperature dependences of the isobaric and isochoric specific heats of hydration water near spherical solute of radius R_s = 5 Å and concave cylindrical surface with R_c = 25 Å with the same water−surface potential U_0 = −1.93 kcal/mol.

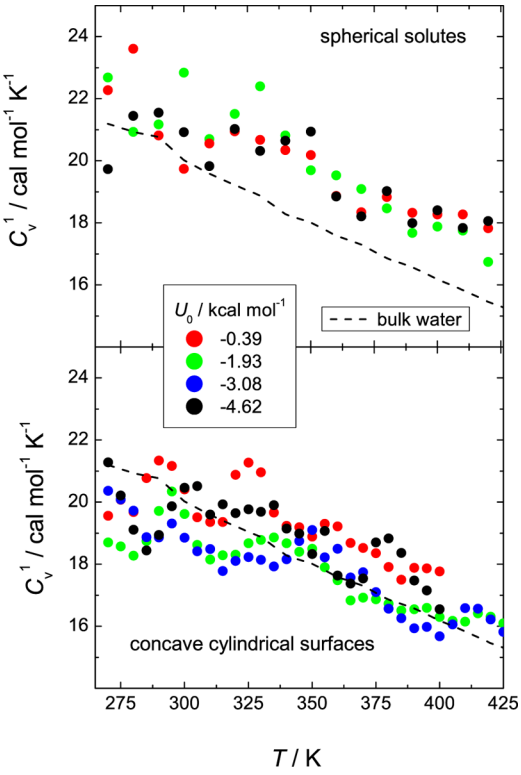

Figure 12. Temperature dependences of the specific heat C_v^1 of hydration water near spherical solutes of radius R_s = 10 Å (upper panel) and near concave cylindrical surfaces with R_c = 25 Å (lower panel) for various water−surface interactions U_0.

which can cause a surface freezing. The values of U_0 used in the present paper cover the majority of this range. The surface curvature has been varied from a negative one for the inner surface of a large cylindrical pore to a positive one for near the surface of small spherical solutes. We have considered mainly the practically relevant thermodynamic states of liquid water, which are close to the liquid−vapor phase transition and not close to the liquid−vapor critical temperature T_c.

The obtained dependences of liquid water density profiles (Figure 1) and of the height of the first density maximum ρ_{max} (Figure 2) on water−surface interaction, surface curvature, and pressure qualitatively agree with the results of the previous studies of water density profiles around various objects.[17−22,24−26,28] In those studies, the water−surface interaction was varied from the case of a "hard wall" to weakly attractive, hydrophobic surfaces with $U_0 > \sim -1$ kcal/mol. In our studies, we have extended the range of U_0 to strongly hydrophilic surfaces. Additionally, we have determined the absolute values of the average density of hydration water ρ^1, which was usually not done in the previous studies of hydration water. This allows the analysis of the liquid water density depletion or enhancement near surfaces. There are areas in the $T-U_0$ plane where the liquid density near a surface is depleted ($\rho^1 < \rho^b$) or enchanced ($\rho^1 > \rho^b$) with respect to the bulk value. Such areas estimated for concave cylindrical surfaces with R_c = 25 Å are shown in the upper panel of Figure 13 by blue and yellow color, respectively. This picture should be a good approximation for the case of planar surfaces, as ρ^1 near surfaces with R_c = 25 Å is close to that estimated at zero surface curvature (Figure 4c).

dx.doi.org/10.1021/jp306781y | J. Phys. Chem. B 2012, 116, 14650−14659

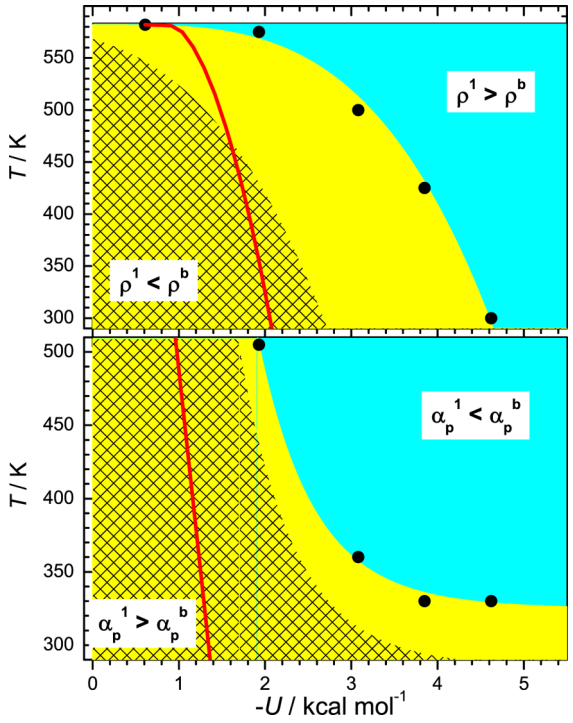

Figure 13. Upper panel: Areas in the $T-U_0$ coordinates, where the density of hydration water is above (blue area) or below (yellow area) the bulk value. Lower panel: Areas in the $T-U_0$ coordinates, where the thermal expansivity of hydration water is below (blue area) or above (yellow area) the bulk value. A sparse pattern indicates a shrinkage of the yellow area for spherical solutes of a radius R_s = 7.5 Å. Red lines correspond to the LJ fluid near planar surfaces.

The *density* of a fluid near a surface is affected by two main factors: missing neighbors effect and fluid−surface interaction. Decrease of the coordination number near a surface causes fluid density depletion, which gains more importance with increasing bulk fluid density. Fluid−surface attraction leads to enchanced fluid density near a surface, and this effect becomes stronger upon decreasing bulk fluid density. Additionally, the density of a *liquid* near weakly attractive surfaces can be strongly affected by the drying transition.[46] The depletion of a liquid density due to the drying transition enhances with approaching the liquid−vapor transition and the drying transition temperature, which is equal to the liquid−vapor critical temperature T_c due to the long-range fluid−surface attractive forces in real systems.[47,48] Drying transition occurs near the surfaces with $U_0 > U_0^c$, where the value U_0^c corresponds to the conditions of a "neutral wall". Near the neutral wall, a fluid being at the critical point has a density near the surface equal to the bulk.[43] In the case of water, $U_0^c \approx -0.61$ kcal/mol.[49] Thus, near hydrophobic surfaces with $U_0 > -0.61$ kcal/mol, liquid density is always depleted due to the formation of a drying layer. Near more hydrophilic surfaces, $\rho^1 = \rho^b$ at some particular temperature T_N^ρ: $T_N^\rho = T_c$ for $U_0 = -0.61$ kcal/mol, and it decreases upon strengthening water−surface interaction. As can be seen from Figure 13, liquid density is depleted even near strongly hydrophilic surfaces whith U_0 of about −4 to −5 kcal/mol at room temperature. This is a result of a missing neighbor effect, i.e., of the worsening of water−water interactions, which remain worse than in the bulk even near strongly hydrophilic surfaces (Figure 7).

The strong effect on the surface curvature on the density of hydration water near hydrophobic surfaces was recognized a long time ago[17] and was confirmed by numerous simulation studies.[18−22,24−26,28] For hydrophobic surfaces, which cause a drying transition of water ($U_0 > -0.61$ kcal/mol), the increase of ρ^1 with decreasing solute size is caused by the effect of a surface curvature on the drying layer.[50,51] Near surfaces with positive curvature, the area of the liquid−vapor interface increases with the thickness of a drying layer, which causes its shrinkage upon decreasing solute size.[46] The effect of solute size on ρ^1 near surfaces which do not cause a drying transition ($U_0 < -0.61$ kcal/mol) originates from the sensitivity of the missing neighbor effect to the surface curvature. Decrease of solute size makes the potential energy of hydration water more negative (Figure 7, middle panel) and causes an increase of ρ^1. This can be easily explained by the fact that the coordination number of molecules in the hydration shell increases, when the solute radius R_s decreases, and it is equal to the bulk value in the limit $R_s \to 0$. The effect of missing neighbors enhances or diminishes near surfaces with negative or positive curvature, respectively. Thus, the decreasing solute size makes the solute effectively more hydrophilic. This qualitatively agrees with the studies of water in closed spherical pores, where the decrease of the pore size makes their inner surface effectively more hydrophobic.[49] The area in the $T-U_0$ plane where liquid water shows density depletion near surfaces shifts toward more hydrophobic surfaces upon decreasing solute size (see the dashed area in the upper panel of Figure 13, estimated for the solutes with R_s = 7.5 Å).

The *thermal expansion coefficient* of hydration water α_p^1 closely correlates with ρ^1 (Figure 6, upper panel), and accordingly, it also strongly depends on the strength of water−surface interaction and on the surface curvature. α_p^1 can be several times larger or smaller than the bulk value near hydrophobic and hydrophilic surfaces, respectively. Near hydrophobic surfaces exhibiting a drying transition ($U_0 > -0.61$ kcal/mol), α_p^1 exceeds the bulk value in the whole temperature range of a liquid state. Near more hydrophilic surfaces ($U_0 < -0.61$ kcal/mol), there is a particular temperature T_N^α, when $\alpha_p^1 = \alpha_p^b$. The dependence $T_N^\alpha(U_0)$ separates the regimes, $\alpha_p^1 > \alpha_p^b$ and $\alpha_p^1 < \alpha_p^b$ (see Figure 13, lower panel). As can be seen from Figure 13, thermal expansivity of hydration water exceeds the bulk value at room temperatures near both hydrophobic and strongly hydrophilic surfaces. α_p^1 decreases with increasing surface curvature. The area in the $T-U_0$ plane, where the thermal expansivity of liquid water near a surface exceeds the bulk value, shifts toward more hydrophobic surfaces upon decreasing solute size (see the dashed area in the lower panel of Figure 13, estimated for the solutes with R_s = 7.5 Å).

Our simulations evidence depletion of density and enhancement of the thermal expansivity of liquid water near various surfaces in a wide temperature range (Figure 13). It is interesting to know whether such a scenario is typical for other fluids or this is just a specific case of water. To answer this question, we have used the simulation studies of LJ fluid in slit-like pores of width 12 σ with various strengths of fluid−surface interaction along the respective pore liquid−vapor coexistence curves. To compare the properties of liquid water and LJ liquid near surfaces quantitatively, we have normalized the critical temperature of LJ fluid and its "neutral" fluid−surface interaction to the respective values for water. The normalized dependence $T_N^\rho(U_0)$ for LJ fluid is shown by the red line in the

dx.doi.org/10.1021/jp306781y | J. Phys. Chem. B 2012, 116, 14650−14659

upper panel of Figure 13. Similarly to water, the density depletion of LJ liquid is observed not only near weakly attractive surfaces, which provoke a drying transition, but also near surfaces, which provoke a wetting transition. Therefore, this phenomenon should be considered as general for fluids. However, as can be seen from Figure 13, this phenomenon is observed in a much wider area in the $T-U_0$ plane for water than for LJ fluid. This can be explained by the fact that water–water interactions suffer more from the missing-neighbor effect due to their strong directionality.

The temperature dependences of α_p^1 for LJ liquid near various surfaces are rather similar to those for liquid water (Figure 14). Theory predicts that the temperature dependence

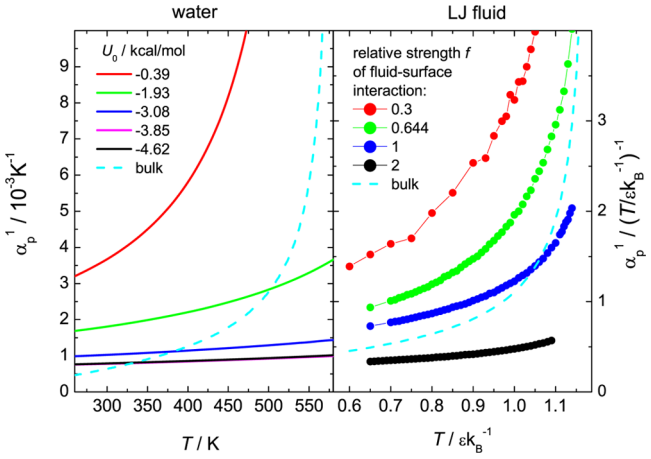

Figure 14. Temperature dependences of the thermal expansion coefficient α_p^1 of hydration water near cylindrical surfaces of radius R_c = 25 Å[29] (left panel) and of LJ liquid near planar surfaces (right panel).

of the liquid density near a surface includes, apart from regular temperature terms, a singular term $\sim(1 - T/T_c)^{0.8}$, which essentially differs from the bulk singular term $\sim(1 - T/T_c)^{0.33}$.[52] This theoretical expectation was confirmed by simulations for water and for LJ fluid.[1] Strictly speaking, the singular term dominates in a close proximity of the critical point only. However, it essentially determines the character of the temperature dependence of the liquid density in a wide temperature range, which extends to the freezing temperature. For example, the dependence $\rho(T)$ for liquid water and for LJ liquid along the liquid–vapor coexistence is close to the cubic parabola far from the surface and becomes linear-like with approaching the surface (Figures 38 and 39 in ref 53 and Figure 8 in ref 54). Obviously, the change of the shape of the dependence $\rho(T)$ affects the thermal expansion coefficient. That is why the similarity of the temperature dependences of α_p^1 for LJ liquid and water is not surprising (Figure 14).

The area in the $T-U_0$ plane where α_p^1 exceeds the bulk value is essentially wider for water in comparison with the case of LJ fluid (Figure 13, lower panel). This reflects the stronger density depletion of liquid water near various surfaces (Figure 13, upper panel), as α_p^1 decreases with increasing ρ^1 (Figure 6, upper panel). However, this does not explain strong extension of the area with $\alpha_p^1 > \alpha_p^b$ toward more hydrophilic surfaces at low temperatures. Specific peculiarity of bulk liquid water is related to the density maximum at 4 °C, where the thermal expansivity is equal to zero. This peculiarity has been attributed to the low-density tetrahedral structures in liquid water, whose concentration increases upon cooling.[1] Formation of such low-density structures is suppressed near a surface, and therefore, this anomaly is absent or much weaker for hydration water, as was assumed in ref 55 and shown in simulations.[56] Thus, the vanishing thermal expansivity of bulk liquid water at low temperatures due to the approaching liquid density maximum seems to be responsible for the quite different shape of the dependences $T_N^\alpha(U_0)$ for LJ fluid and for water: for LJ fluid, T_N^α drops sharply below the freezing temperature upon strengthening fluid–surface interaction, whereas, for water, it remains above the freezing temperature even for strongly hydrophilic surfaces.

The constant pressure specific heat of hydration water C_p^1 increases upon weakening water–surface interaction: it can be slightly below the bulk value near strongly hydrophilic surfaces, and it essentially exceeds the bulk value near hydrophobic surfaces (Figure 10). This observation well agrees with the experiments on dissolution of organic molecules in liquid water[9,10] and with the simulation studies of C_p^1 near small hydrophobic solutes.[33−35] C_p^1 is found to be practically not sensitive to the surface curvature (Figure 11, upper panel). To understand the behavior of C_p^1, it is important to know both C_v^1 and α_p^1, as $C_p^1 = C_v^1 + VT\alpha_p^1(dp/dT)_V$. We have found that the constant volume specific heat of liquid water practically does not change near surfaces: C_v^1 is close to the bulk value near various surfaces (Figure 12, lower panel) and only slightly increases with decreasing solute size (Figure 11, lower panel). Therefore, an increase of C_p^1 near hydrophobic surfaces originates from a drastic increase of α_p^1. Independence of C_p^1 on the surface curvature (Figure 12, upper panel) should be atributed to the opposite effect of surface curvature on the two constituents of C_p^1. Indeed, C_v^1 increases (Figure 12, lower panel), whereas α_p^1 decreases (Figure 12, lower panel) upon decreasing solute size.

V. CONCLUSION

Density depletion and increasing thermal expansivity are the main effects of various surfaces on liquid water. These effects gain more importance upon cooling, upon weakening water–solute interaction, and upon increasing solute size. The obtained regularities are general for fluids and agree with the theoretical expactations, but they are especially strong for water, as directional H-bonding strongly suffers from the presence of a surface. Increasing thermal expansivity of liquid water near surfaces causes an increase of its constant pressure heat capacity C_p, and this effect is especially strong near hydrophobic surfaces. This conclusion is supported by the insensitivity of the constant volume heat capacity C_v of water near surfaces to the strength of water–surface interaction.

AUTHOR INFORMATION

Corresponding Author

*E-mail: alla.oleynikova@tu-dortmund.de.

Notes

The authors declare no competing financial interest.

ACKNOWLEDGMENTS

The authors gratefully acknowledge financial support form DFG (grant OL 314/1).

REFERENCES

(1) Brovchenko, I.; Oleinikova, A. *Interfacial and Confined Water*; Elsevier: Amsterdam, The Netherlands, 2008; p 320.

(2) Doster, W.; et al. *Phys. Rev. Lett.* **2010**, *104*, 098101.
(3) Shi, Q.; et al. *J. Phys. Chem. C* **2012**, *116*, 3910−3917.
(4) Derjaguin, B. V.; Karasev, V. V.; Khromova, E. N. *J. Colloid Interface Sci.* **1986**, *109*, 586−587.
(5) Etzler, F. M.; Fagundus, D. M. *J. Colloid Interface Sci.* **1987**, *115*, 513−519.
(6) Takei, T.; et al. *Colloid Polym. Sci.* **2000**, *278*, 475−480.
(7) Xu, S.; Simmons, G. C.; Scherer, G. W. *Mater. Res. Soc. Symp. Proc.* **2004**, *790*, 85−91.
(8) Valenza-II, J. J.; Scherer, G. W. *Cem. Concr. Res.* **2005**, *35*, 57−66.
(9) Edsall, J. T. *J. Am. Chem. Soc.* **1935**, *57*, 1506−1507.
(10) Makhatadze, G.; Privalov, P. *J. Mol. Biol.* **1990**, *213*, 375−384.
(11) Jensen, T. R.; et al. *Phys. Rev. Lett.* **2003**, *90*, 086101.
(12) Poynor, A.; et al. *Phys. Rev. Lett.* **2006**, *97*, 266101.
(13) Mezger, M.; et al. *Proc. Natl. Acad. Sci. U.S.A.* **2006**, *103*, 18401−18404.
(14) Cheng, L.; et al. *Phys. Rev. Lett.* **2001**, *87*, 156103.
(15) Mancinelli, R.; et al. *J. Phys. Chem. B* **2009**, *113*, 16169−16177.
(16) Mancinelli, R.; Bruni, F.; Ricci, M. A. *J. Phys. Chem. Lett.* **2010**, *1*, 1277−1282.
(17) Stillinger, F. H. *J. Solution Chem.* **1973**, *2*, 141−158.
(18) Pratt, L. R.; Pohorille, A. *Proc. Natl. Acad. Sci. U.S.A.* **1992**, *89*, 2995−2999.
(19) Hummer, G.; Garde, S. *Phys. Rev. Lett.* **1998**, *80*, 4193−4196.
(20) Lum, K.; Chandler, D.; Weeks, J. D. *J. Phys. Chem. B* **1999**, *103*, 4570−4577.
(21) Huang, D. M.; Geissler, P. L.; Chandler, D. *J. Phys. Chem. B* **2001**, *105*, 6704−6709.
(22) Ashbaugh, H. S.; Paulaitis, M. E. *J. Am. Chem. Soc.* **2001**, *123*, 10721−10728.
(23) Mamatkulov, S.; Khabibullaev, P.; Netz, R. *Langmuir* **2004**, *20*, 4756−4763.
(24) Rajamani, S.; Truskett, T. M.; Garde, S. *Proc. Natl. Acad. Sci. U.S.A.* **2005**, *102*, 9475−9480.
(25) Mittal, J.; Hummer, G. *Proc. Natl. Acad. Sci. U.S.A.* **2008**, *105*, 20130−20135.
(26) Sarupria, S.; Garde, S. *Phys. Rev. Lett.* **2009**, *103*, 037803.
(27) Chau, P.-L. *Mol. Phys.* **1996**, *89*, 1033−1055.
(28) Huang, D. M.; Chandler, D. *J. Phys. Chem. B* **2002**, *106*, 2047−2053.
(29) Oleinikova, A.; Brovchenko, I.; Winter, R. *J. Phys. Chem. C* **2009**, *113*, 11110−11118.
(30) Brovchenko, I.; et al. *J. Chem. Phys.* **2008**, *129*, 195101.
(31) Brovchenko, I.; Burri, R.; Krukau, A.; Oleinikova, A. *Phys. Chem. Chem. Phys.* **2009**, *11*, 5035−5040.
(32) Brovchenko, I.; Andrews, M. N.; Oleinikova, A. *Phys. Chem. Chem. Phys.* **2010**, *12*, 4233−4238.
(33) Sharp, K. A.; Madan, B. *J. Phys. Chem. B* **1997**, *101*, 4343−4348.
(34) Madan, B.; Sharp, K. *J. Phys. Chem. B* **1997**, *101*, 11237−11242.
(35) Paschek, D. *J. Chem. Phys.* **2004**, *120*, 10605−10617.
(36) Oleinikova, A.; Brovchenko, I.; Singh, G. *Europhys. Lett.* **2010**, *90*, 36001.
(37) Jorgensen, W. L.; et al. *J. Chem. Phys.* **1983**, *79*, 926−935.
(38) Brovchenko, I.; Geiger, A.; Oleinikova, A. *Phys. Chem. Chem. Phys.* **2004**, *6*, 1982−1987.
(39) Brovchenko, I.; Oleinikova, A. *J. Phys. Chem. B* **2010**, *114*, 16494−16502.
(40) Brovchenko, I.; Geiger, A. *J. Mol. Liq.* **2002**, *96*, 195−206.
(41) Brovchenko, I.; Oleinikova, A. *J. Phys. Chem. C* **2007**, *111*, 15716−15725.
(42) Brovchenko, I.; Geiger, A.; Oleinikova, A. *Eur. Phys. J. B* **2005**, *44*, 345−358.
(43) Maciolek, A.; Evans, R.; Wilding, N. B. *J. Chem. Phys.* **2003**, *119*, 8663−8675.
(44) Oleinikova, A.; Brovchenko, I. *Phys. Rev. E* **2007**, *76*, 041603.
(45) Wagner, W.; Pruss, A. *J. Phys. Chem. Ref. Data* **2002**, *31*, 387−535.
(46) Dietrich, S. In *Phase Transitions and Critical Phenomena*; Domb, C., Lebowitz, J. L., Eds.; Academic Press: London, 1988; Vol. *12*, pp 1−218.
(47) Nightingale, M. P.; Saam, W. F.; Schick, M. *Phys. Rev. B* **1984**, *30*, 3830−3840.
(48) Ebner, C.; Saam, W. F. *Phys. Rev. B* **1987**, *35*, 1822−1834.
(49) Brovchenko, I.; Oleinikova, A. *Phys. Chem. B* **2011**, *115*, 9990−10000.
(50) Bieker, T.; Dietrich, S. *Physica A* **1998**, *252*, 85−137.
(51) Stewart, M.; Evans, R. *J. Phys.: Condens. Matter* **2005**, *17*, S3499.
(52) Binder, K. In *Phase Transitions and Critical Phenomena*; Domb, C., Lebowitz, J. L., Eds.; Academic Press: London, 1983; Vol. *8*, pp 1−144.
(53) Brovchenko, I.; Oleinikova, A. In *Handbook of Theoretical and Computational Nanotechnology*; Rieth, M., Schommers, W.; American Scientific Publishers: Stevenson Ranch, CA, 2006; Vol. *9*, Chapter 3, pp 109−206.
(54) Brovchenko, I.; Geiger, A.; Oleinikova, A. *J. Phys.: Condens. Matter* **2004**, *16*, S5345−S5370.
(55) Hiebl, M.; Maksymiv, R. *Biopolymers* **1991**, *31*, 161−167.
(56) Brovchenko, I.; Oleinikova, A. *J. Chem. Phys.* **2007**, *126*, 214701.
(57) Kalinichev, A.; Gorbaty, Y.; Okhulkov, A. *J. Mol. Liq.* **1999**, *82*, 57−72.